MOLECULAR PHYSICS REPORTS 10 (1995) 26-47

COMPUTER-AIDED DESIGN OF FERROELECTRIC LIQUID CRYSTALS

MATTHEW A. GLASER[1], VALERIY V. GINZBURG[1], NOEL A. CLARK[1], EDGARDO GARCIA[2], DAVID M. WALBA[2], RAINER MALZBENDER[3]

[1] *Condensed Matter Laboratory, Department of Physics, University of Colorado, Boulder, Colorado 80309, U.S.A.*
[2] *Department of Chemistry and Biochemistry, University of Colorado, Boulder, Colorado 80309, U.S.A.*
[3] *Displaytech, Inc., Boulder, Colorado 80301, U.S.A.*

ABSTRACT: We have formulated a new computational method for the prediction of the spontaneous polarization density P in ferroelectric liquid crystals (FLCs) from atomistic models of molecular structure. Our theoretical model combines the zig-zag model of smectic C ordering [7] with the modular mean-field theory formalism of Photinos et al. [10], and makes use of specially designed hybrid Monte Carlo methods for evaluating statistical averages. We examine a number of test cases, and demonstrate that this model yields reliable semi-quantitative predictions of P. Our results provide strong support for the Boulder model [6] for P. Moreover, our approach enables detailed studies of the molecular origins of P, and should prove to be a useful tool for the design of new FLC materials.

I. INTRODUCTION

Liquid crystalline materials are of interest both as unique phases of matter and as components of electro-optic devices. Despite increased activity in the field, and a market for liquid crystal devices approaching $ 5 billions/year, the design of new liquid crystal materials remains as much an art as a science, proceeding by trial and error aided by a plethora of poorly understood empirical rules.

The potential for computer simulation and theory to illuminate this situation is great. Despite their complexity, liquid crystal molecules (typical examples of which are shown in Figure 3) are small by macromolecular standards, and the difficulties inherent in the modelling of such systems are correspondingly reduced. Nevertheless, significant challenges remain, owing to the complexity of liquid crystal structure and interactions, the high degree of cooperativity present in the more ordered liquid crystal phases, and the broad range of timescales that characterize the microscopic dynamics in these materials. Although systematic theoretical studies have been carried out for simple model systems such as hard spherocylinders and soft ellipsoids (see, for example, [1]), only a limited number of studies of realistic liquid crystal models have been attempted [2].

The intrinsic difficulty of computing liquid crystal properties from first principles depends strongly on the particular property being considered. Most challenging, perhaps, is the calculation of the phase diagram. To date, no convincing calculation of the phase behavior of an atomistic model liquid crystal has been reported. The scale of some problems can be greatly reduced by the application of detailed mean-field theories or cluster approximations. However, such calculations have primarily been applied to the interpretation of NMR measurements, and their potential range of applicability has only begun to be explored.

We have recently started to develop techniques for the first-principles calculation of liquid crystal properties, utilizing large-scale computer simulation, cluster approximations, and mean-field theory. In this paper, we describe our first steps toward the goal stated in the title, namely the directed, computer-aided design of ferroelectric liquid crystals (FLCs). Specifically, we present a novel mean-field model for ferroelectric polarization density in smectic C^* liquid crystals, and report some preliminary results obtained using this model.

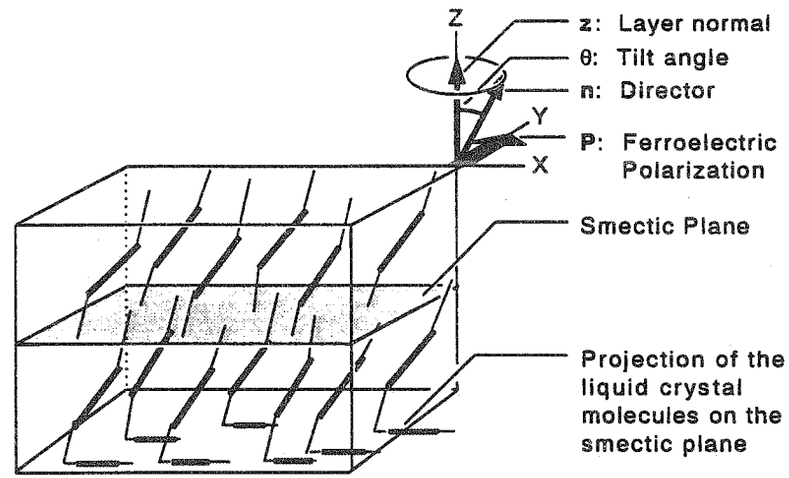

Fig. 1. Geometry of the smectic C and C^* phases. Liquid crystal molecules are arranged in layers, and are oriented, on average, along the director, $\hat{\mathbf{n}}$, which is tilted by an angle θ with respect to the layer normal $\hat{\mathbf{z}}$. In the smectic C^* phase, a spontaneous ferroelectric polarization appears in the direction normal to the plane defined by $\hat{\mathbf{n}}$ and $\hat{\mathbf{z}}$ (the tilt plane).

Liquid crystals can be broadly defined as phases of matter having order intermediate between that of isotropic fluids and three-dimensional crystals. The geometry of the liquid crystal phase discussed in this paper, the smectic C phase, is displayed in Figure 1. This phase is characterized by *molecular orientational* order (molecular long axes align, on average, along a particular direction, specified by the *director*, $\hat{\mathbf{n}}$), *one-dimensional translational* order (molecules are arranged in layers perpendicular to the z axis), and *tilt* order (molecules are tilted, on average, with respect to the layer

normal $\hat{\mathbf{z}}$, so that $\hat{\mathbf{n}}$ and $\hat{\mathbf{z}}$ are not collinear). Only short-range translational order is present within each layer, so this phase can be thought of as a stack of two-dimensional liquid layers. In fact, smectic C liquid crystals are *monoclinic fluids*! Moreover, as discussed below, the low symmetry of this phase implies that smectic C liquid crystals composed of *chiral* (non-centrosymmetric) molecules (denoted smectic C^*) are *ferroelectric fluids* [3]. The current high level of interest in FLCs is, in large part, due to the invention of fast, bistable electo-optic devices (surface-stabilized FLCs, or SSFLCs) based on these materials [4].

The possibility of ferroelectricity in liquid crystals was first recognized by Meyer [3], who advanced a simple symmetry argument predicting that the smectic C^* phase should be ferroelectric. The essence of his argument is as follows: an ordinary (non-chiral) smectic C phase exhibits mirror reflection (σ) symmetry with respect to the tilt plane (the plane defined by $\hat{\mathbf{n}}$ and $\hat{\mathbf{z}}$) and twofold rotational (C_2) symmetry about the normal to the tilt plane $\hat{\mathbf{y}}$ (a consequence of the $\hat{\mathbf{n}} \rightarrow -\hat{\mathbf{n}}$ symmetry of the smectic C phase). The introduction of chiral molecules destroys the mirror reflection symmetry of the phase, which leads to polar order along the axis normal to the tilt plane (the y axis). Polar order does not develop along the x and z directions because local C_2 symmetry is still present in the smectic C^* phase. If the chiral molecule contains polar groups, then the polar ordering will result in a macroscopic ferroelectric polarization density $\mathbf{P} = P_y\hat{\mathbf{y}}$. (In the following, we will refer only to the *scalar* polarization density $P \equiv P_y$.) The smectic C^* phase has only *local* C_2 symmetry because this phase generally exhibits a helical twist of the tilt direction about the layer normal. This leads to $P = 0$ for bulk smectic C^* samples. However, if the helix is suppressed (e.g. by surface interactions, as in SSFLCs [4]), then a nonzero P is manifested.

The foregoing symmetry argument for P simply predicts that a nonzero P should be present, but provides no information about the magnitude or sign of P (by convention, P is positive if it is along $\hat{\mathbf{z}} \times \hat{\mathbf{n}}$ and negative otherwise). The measured values of P vary widely from material to material, ranging from immeasurably small ($|P| < 0.1$ nC/cm^2) to very large ($|P| = 1100$ nC/cm^2). Despite a wealth of empirical information, the features of molecular structure and microscopic ordering responsible for such wide variability in $|P|$ remain obscure. An understanding of the variation of P with molecular structure requires a microscopic theory for smectic C^* ordering.

One possible microscopic mechanism for ferroelectric polarization in FLCs has been sketched by de Gennes (see [5], p. 320). He considered molecules having the symmetry of a fish, i.e. with a distinct head and tail and a distinguishable front and back. In the smectic C phase, each molecule prefers to be at a certain angle with respect to the layer normal. Moreover, due to the monoclinic symmetry of the smectic C phase, the molecule has an anisotropic distribution of orientations about its long axis. In de Gennes' example, a fish-shaped molecule prefers to have its back near the center

of the layer. Because there is no symmetry operation of the smectic C phase that transforms a molecule with its back near the center of the layer to one with its front near the center of the layer, the probabilities of these two molecular orientations will be different in general. Thus, even the achiral smectic C phase possesses polar orientational ordering. This polar ordering is not manifested in a macroscopic ferroelectric polarization, however, because of the mirror reflection symmetry of the phase. A given molecular configuration and its mirror image with respect to the tilt plane make contributions to P of equal magnitude but of opposite sign and are present with equal probability in the smectic C phase, so $P = 0$ overall. This is not true in the smectic C^* phase, however, because the mirror image of any configuration of a chiral molecule is a molecule having the opposite handedness, which is not present in an enantiomerically pure smectic C^* material. Thus, we no longer have $P = 0$. Returning to de Gennes' example, the two orientations (back near center of layer and front near center of layer) of a *chiral* fish with an electric dipole moment pointing out of its right eye (i.e. with distinguishable right and left sides) make contributions to P of equal magnitude and opposite sign, but are present with different probabilities, and so $P \neq 0$. (Notice that two molecular configurations related by the C_2 symmetry operation make contributions to P having the same sign and magnitude.) This microscopic mechanism for P does not require any special intermolecular interactions associated with the chiral groups in the molecule. P arises as a straightforward consequence of the polar orientational ordering *already present* in the achiral smectic C phase.

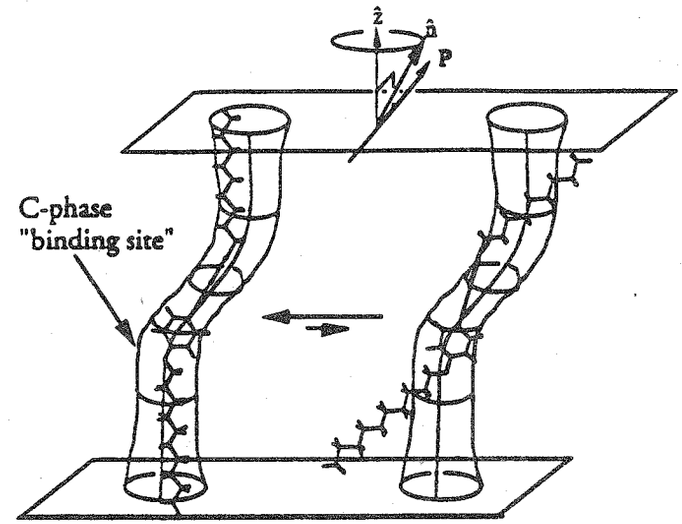

Fig. 2. Schematic depiction of the Boulder model for ferroelectric polarization in the smectic C^* phase. Two orientational states of an FLC molecule within the smectic C "binding site" are shown, illustrating how the monoclinic symmetry of the mean-field potential produces polar orientational anisotropy about the molecular long axis.

The Boulder model [6] combines de Gennes' argument with the *zig-zag* hypothesis [7], the assumption that molecular cores are, on average, more tilted than tails in the smectic C phase, in order to construct a microscopic model capable of specific predictions regarding P. In this model, the interactions of a given molecule with surrounding molecules are represented by an effective mean-field potential ("binding site") which has the form of a bent cylinder with repulsive walls. As shown in Figure 2, the zig-zag form of this potential breaks the rotational symmetry of the molecular orientational distribution about the director, and leads to a net ferroelectric polarization density if the molecule is chiral. The physical inequivalence of core and tail regions implies that, on average, they will have different tilt angles. The preponderance of experimental evidence seems to support the assumption that cores are more tilted than tails. Note that the mean-field potential in the Boulder model is assumed to be *achiral* (i.e. mirror-symmetric with respect to the tilt plane). The chirality responsible for polar ordering is manifested at the single-molecule level in this model, and molecular chirality is assumed not to lead to any collective chiral ordering. Of course, the presence of a helix is a manifestation of collective chiral ordering, but the fact that the helical pitch is large (equal to many smectic layer spacings) for most smectic C^* materials is evidence that such collective effects are weak. To date, the Boulder model has been used primarily as a conceptual aid, and has been used with some success to rationalize the observed sign (and to a lesser extent the magnitude) of P for a variety of smectic C^* materials [6]. The model described in this article represents an attempt to turn the Boulder model into a computational tool capable of yielding quantitative predictions.

Two other microscopic models for P are of note. In contrast to the Boulder model, the theory of Osipov and Pikin [8] is based on the assumption that specific chiral interactions are responsible for ferroelectricity in the smectic C^* phase (i.e. that the microscopic ordering of the smectic C^* phase differs fundamentally from that of the smectic C phase). Very recently, Photinos and Samulski have argued that the microscale segregation of chemically distinct parts of liquid crystal molecules in the smectic C phase, combined with a zig-zag molecular shape, can lead to rotational anisotropy about the nematic director, and hence produce nonzero P for chiral molecules [9]. Like the Boulder model, this model assumes that there is no fundamental difference in the microscopic ordering of the smectic C and C^* phases. As far as we know, neither theory has yielded quantitative predictions of P for specific materials.

II. A MEAN-FIELD MODEL FOR THE SMECTIC C PHASE

As mentioned in the introduction, we attempted to turn the Boulder model into a computational tool capable of quantitative predictions of P for FLCs. In doing this we tried to introduce the minimum number of arbitrary assumptions. We assume

a simple form for the mean-field potential experienced by a single molecule in the smectic C phase, and carry out a statistical average over all orientations and conformations of a molecule subject to this potential, with a specific representation of the molecular structure and intramolecular interactions. We further assume that smectic C ordering is *universal* in the sense that a uniform parametrization of the mean-field potential can be used for all smectic C materials. The limitations of this assumption will be discussed in more detail below. The molecular model and interaction potential used in these studies are described in Section III, and the methods used for performing statistical averages are discussed in Section IV. In this section we describe the form of the mean-field potential used in this work.

To describe the mean-field potential experienced by a single molecule in the smectic C phase, we adopted the modular mean-field formalism of Photinos et al. [10], which is an extension of earlier work by Marcelja [11] and Luckhurst and co-workers [12]. This theory is a generalization of the Maier-Saupe theory of nematics [5] to flexible molecules. The Photinos theory represents the potential of mean torque as a sum of orientational potentials acting on individual rigid molecular segments, together with nearest-neighbour segment interaction terms. This theory has been used with considerable success to model NMR measurements on nematic liquid crystals and flexible solutes in nematic solvents [10].

For a simple chain molecule with a discrete set of conformations, the potential of mean torque in the nematic phase has the form

$$V_{mf}(\omega,n) = -\omega_0 \sum_{i=1}^{N_s} P(\hat{\mathbf{s}}_i,\hat{\mathbf{s}}_i;\hat{\mathbf{n}}) - \omega_1 \sum_{i=1}^{N_s-1} P(\hat{\mathbf{s}}_i,\hat{\mathbf{s}}_{1+1};\hat{\mathbf{n}}), \tag{1}$$

where ω denotes the orientation of the molecule, n is a conformation index, $\hat{\mathbf{s}}_i$ is a unit vector along the ith rigid molecular segment (generally taken to coincide with a nearest-neighbour bond), N_s is the number of segments, w_0 and w_1 are coupling constants, and

$$P(\hat{\mathbf{s}}_i,\hat{\mathbf{s}}_j;\hat{\mathbf{n}}) = \frac{1}{2}[3(\hat{\mathbf{s}}_i\cdot\hat{\mathbf{n}})(\hat{\mathbf{s}}_j\cdot\hat{\mathbf{n}}) - \hat{\mathbf{s}}_i\cdot\hat{\mathbf{s}}_j]. \tag{2}$$

Here, as above, $\hat{\mathbf{n}}$ is the nematic director. As discussed by Photinos et al. [10], three cases can be distinguished: (1) the uncorrelated bond model ($w_1 = 0$); (2) the chord model ($w_1 = w_0$); and (3) the biaxial block model ($w_1 \neq w_0$). This general form for the potential of mean torque is dictated by the requirement of $\hat{\mathbf{n}} \rightarrow -\hat{\mathbf{n}}$ symmetry within the framework of a second-rank tensor dependence [10].

With this form of mean-field potential, the average of any quantity $A(\omega, n)$ can be obtained by averaging over all orientations and conformations,

$$\langle A\rangle = Z^{-1}\sum_n \int d\omega\, A(\omega,n)G(n)\exp\{-\beta[V_{mf}(\omega,n)+V_{int}(n)]\}. \quad (3)$$

Here $\beta = 1/(k_BT)$, $V_{int}(n)$ is the intramolecular potential energy for conformation n, $G(n)$ is a kinetic metric correction [10], and

$$Z = \sum_n \int d\omega\, G(n)\exp\{-\beta[V_{mf}(\omega,n)+V_{int}(n)]\}. \quad (4)$$

is the configurational partition function.

We decided to use the biaxial block model in the present study because it is easily extended to branched molecules, and because it has been found to give the best overall description of the ordering of flexible solutes in nematic solvents [10]. We extended this model in several respects to construct a mean-field theory appropriate for smectic C materials and to remove the restriction to a discrete set of conformational states. (As described in the Section IV, we used a fully flexible molecular model). Our mean-field potential can be written in the form

$$V_{mf}(\mathbf{r}^N) = -\sum_{i=1}^{N_s}\omega_{0i}P(\hat{\mathbf{s}}_i,\hat{\mathbf{s}}_i;\hat{\mathbf{n}}_t) - \sum_{i,j}\omega_{1ij}P(\hat{\mathbf{s}}_i,\hat{\mathbf{s}}_j;\hat{\mathbf{n}}_t) - \omega_{0c}P(\hat{\mathbf{s}}_c,\hat{\mathbf{s}}_c;\hat{\mathbf{n}}_c) \quad (5)$$

where the first sum runs over all bond segments in both liquid crystal tails, the second sum runs over all nearest-neighbour pairs of bond segments in both tails, and the third term is an orientational potential that couples to the liquid crystal core, with $\hat{\mathbf{s}}_c$ a unit vector parallel to the core end-to-end vector. $\hat{\mathbf{n}}_t$ and $\hat{\mathbf{n}}_c$ are the reference directors for tail segments and the core segment, respectively. Zig-zag ordering can be imposed on the molecule by choosing $\hat{\mathbf{n}}_t$ to be inclined with respect to $\hat{\mathbf{n}}_c$. Different coupling constants are assigned to each segment and to each segment pair to account for the existence of a number of chemically distinct bond types in typical FLC materials. The molecular core is defined as the minimal contiguous (connected) group of atoms containing all rings.

In this case, we have a slightly different expression for the average of a quantity $A(\mathbf{r}^N)$,

$$\langle A\rangle = Z^{-1}\int d\mathbf{r}^N A(\mathbf{r}^N)\exp\{-\beta[V_{mf}(\mathbf{r}^N)+V_{int}(\mathbf{r}^N)]\} \quad (6)$$

where

$$Z = \int d\mathbf{r}^N \exp\{-\beta[V_{mf}(\mathbf{r}^N)+V_{int}(\mathbf{r}^N)]\} \quad (7)$$

The form of the intramolecular potential energy $V_{int}(\mathbf{r})^N$ is detailed in the next section.

To simplify the expression for the potential of mean torque, we have assumed that the coupling constants depend only on the segment lengths:

$$\begin{aligned}\omega_{0}|\mathbf{s}_i|^2\\ \omega_{1ij} = W_1|\mathbf{s}_i||\mathbf{s}_j|\\ \omega_{0c} = W_{0c}|\mathbf{s}_c|^2,\end{aligned} \quad (8)$$

where $\mathbf{s}_i$ is the ith bond vector and $\mathbf{s}_c$ is the core end-to-end vector. Finally, to reduce the number of effective parameters, we chose $W_1/W_0 = 0.85$ (this ratio was found to be optimal for alkanes dissolved in nematic solvents [10]) and $W_{0c} = W_0$.

With these simplifying assumptions, the model depends only on two parameters, the orientational coupling constant, W_0, and the tilt angle of the core reference director relative to that of the tails, $\theta_{rel} = \cos^{-1}(\hat{\mathbf{n}}_c\cdot\hat{\mathbf{n}}_t)$. If cores are assumed to be more tilted than tails in the smectic C phase, then $\hat{\mathbf{n}}_t\times\hat{\mathbf{n}}_c \parallel \hat{\mathbf{z}}\times\hat{\mathbf{n}}$, so that P in the direction of $\hat{\mathbf{n}}_t\times\hat{\mathbf{n}}_c$ is positive.

A few comments are in order regarding the assumptions that have been made in deriving this mean-field potential. First of all, note that we are using a *purely orientational* potential. A proper mean-field potential for a smectic would also depend on the z coordinate of the molecular center of mass. The potential that we have written down represents the effective mean-field potential obtained by integrating out the z-dependence. Because P depends only on the effective single-molecule conformational-orientational distribution (and not on the z distribution), such a procedure is justified. Secondly, note that the key physical assumption is the assumption of zig-zag ordering, which is introduced into the model via independent core and tail reference directors. This is the sole source of rotational anisotropy in the model. Each term in the potential is invariant under rotation about the corresponding reference director, but the introduction of two reference directors leads to a global orientational symmetry breaking. Thirdly, note that our model does not distinguish between smectic C and smectic C^* liquid crystals. The mean-field potential is achiral (i.e. invariant under mirror reflection in the plane defined by $\hat{\mathbf{n}}_t$ and $\hat{\mathbf{n}}_c$), which implies that chirality is manifested only at the single-molecule level in our model. Finally, an underlying assumption of our model is that smectic C ordering is *universal* in the sense that a uniform parametrization of the mean-field potential can be applied to a variety of FLC materials. This assumption is necessary if our model is to have predictive power. The remaining assumptions are made in the interest of simplicity, both to reduce the number of arbitrary parameters in the model and to facilitate its application to a wide variety of FLC materials in a uniform and automatic way.

III. MOLECULAR MODEL AND FORCE FIELD

The molecular model used in this study is a hybrid between the all-atom and effective-atom representations of molecular structure. We use an all-atom representation for aromatic rings (i.e. hydrogen atoms are included explicitly) and an effective-atom

representation for aliphatic tails (CH_1, CH_2, and CH_3 groups are treated as single spherically symmetric interaction sites). The effective-atom representation greatly reduces the computational effort required to carry out statistical averages by reducing the number of pair interactions that need to be computed (by at least a factor of 4). While this approximation works reasonably well for liquid alkanes [13], the corresponding approximation for benzene appears to be too crude in that it grossly misrepresents the molecular shape and charge distribution [14]. For this reason our molecular model retains explicit hydrogens on aromatic rings.

The intramolecular interactions were represented by a specially designed empirical force field, the *hybrid force field* (HFF), which is currently being developed at the University of Colorado. We are developing this force field in order to correct some of the most serious shortcomings of standard empirical force fields and to represent intramolecular interactions within the hybrid representation described above. HFF can be written in the form

$$V_{\mathrm{HFF}}(\mathbf{r}^N) = V_b + V_a + V_t + V_i + V_{\mathrm{vdw}} + V_{\mathrm{coul}}, \tag{9}$$

where the various terms correspond to bond stretching, bond angle bending, dihedral torsion, improper torsion, van der Waals, and Coulomb interactions, respectively. We chose fairly standard functional forms for the individual terms in V_{HFF}, but developed our own parametrization in order to represent intramolecular interactions in liquid crystals faithfully. To this end we carried out extensive *ab initio* quantum chemical calculations to derive accurate equilibrium geometries and torsional potentials. HFF will be described in detail in a subsequent publication [15].

For our single-molecule simulations, we found it necessary to introduce an additional *elongation* potential, V_{elong}, to prevent molecules from folding due to intramolecular van der Waals attractions. The tendency to fold is an artifact of carrying out simulations in vacuum, in which case the intramolecular interactions are unscreened by intermolecular interactions. V_{elong} has the form

$$V_{\mathrm{elong}} = -\alpha |\mathbf{r}_{\mathrm{ee}}|, \tag{10}$$

where $\mathbf{r}_{\mathrm{ee}}$ is the molecular end-to-end vector (the vector joining the endpoints of the two tails). For the simulations reported here, we took $\alpha = 0.15$ kcal/mole/Å, which is the value obtained from a crude estimate of the decrease in the van der Waals energy of an alkane chain upon folding.

IV. COMPUTATIONAL METHODOLOGY

Because of the large number of degrees of freedom for even a single liquid crystal molecule, carrying out the statistical average of equation 6 is a nontrivial task, particularly for a fully flexible molecular model. For this reason we resorted to computer simulation for the evaluation of statistical averages. In this study, we adopted the hybrid Monte Carlo (HMC) method [16]. In the next few paragraphs we briefly describe this method and discuss other details of the simulations.

The HMC method was originally developed in the context of lattice field theory [16], but has recently found application to problems in condensed matter physics [17]. HMC is a hybrid of microcanonical molecular dynamics (MD) and canonical Monte Carlo (MC), in which short MD trajectories are generated to propose trial moves for a MC procedure. A single HMC move consists of the following three steps:

1. Given the current configuration $\mathbf{r}^N$, sample new momenta $\mathbf{p}^N$ from a Maxwellian distribution,

$$\rho_K(\mathbf{p}^N) = Z_K^{-1} \exp\left(-\beta \sum_{i=1}^{N} \frac{|\mathbf{p}_i|^2}{2m_i} \right) \tag{11}$$

where the m_i are the particle masses and Z_K is a normalization factor.

2. Evolve the system forward in time for N^{MD} MD timesteps of size Δt according to the equations of motion generated by a *guidance* Hamiltonian H_G, to produce a new set of coordinates and momenta $\mathbf{r}'^N, \mathbf{p}'^N$).

3. Accept the new configuration with probability

$$P_{\mathrm{acc}} = \min[1, \exp(-\beta \Delta H)] \tag{12}$$

where $\Delta H = H(\mathbf{r}'^N, \mathbf{p}'^N) - H(\mathbf{r}^N, \mathbf{p}^N)$ is the change in the *true* Hamiltonian H. Otherwise, reset the coordinates to $\mathbf{r}^N$.

Provided that the MD algorithm used to integrate the equations of motion is *time reversible* and *area-preserving* ($|J| = |\partial(\mathbf{r}'^N, \mathbf{p}'^N) / \partial(\mathbf{r}^N, \mathbf{p}^N)| = 1$), it is easy to show that the HMC procedure satisfies detailed balance and generates configurations governed by a canonical distribution [16]. MD algorithms that satisfy these criteria are described below. The HMC method depends on two parameters, N_{MD} and Δt, which need to optimized in general. In practice, the optimization with respect to N_{MD} is the most important. Notice that if the equations of motion were integrated exactly, and if $H_G = H$, the *discretization error* ΔH would be zero, and thus P_{acc} would be unity (the Hamiltonian is a constant of the motion). The use of a discrete-time approximation for the dynamical evolution of the system (and/or the use of a guidance Hamiltonian $H_G \neq H$) leads to a finite discretization error and an acceptance rate smaller than unity.

HMC resembles canonical dynamics [18, 19] in that it uses MD to generate a canonical ensemble. What are the advantages of HMC? Firstly, HMC is guaranteed to yield a canonical ensemble, whereas canonical dynamics is known to exhibit nonergodic behavior, and hence fail to produce a canonical distribution, in some cases [19].

HMC is, therefore, more reliable than canonical dynamics. More importantly, HMC is a much more flexible technique than canonical MD. Some indication of the flexibility of HMC is reflected in the possibility (alluded to above) of generating the dynamics from a guidance Hamiltonian H_G different from the true system Hamiltonian H. It is even possible to use a guidance Hamiltonian with an explicit time dependence, provided that the time variation is symmetric over the interval of the HMC trajectory. In our simulations of FLC materials, we used an HMC scheme in which some part of the potential energy varies sinusoidally between the true potential energy and a modified potential energy over the course of an HMC trajectory,

$$V_G(\mathbf{r}^N,t) = V(\mathbf{r}^N) + \frac{1}{2}\left[1 - \cos\left(\frac{2\pi t}{N_{MD}\Delta t}\right)\right][V_{\text{mod}}(\mathbf{r}^N) - V(\mathbf{r}^N)]\,. \tag{13}$$

This variant of HMC, which we call *potential variation* HMC (PVHMC), enables one to dynamically remove large energy barriers separating disjoint regions of configuration space during the course of a single HMC trajectory, thereby greatly increasing the barrier-crossing rate in some cases. We have found PVHMC to be very effective in improving conformational sampling in simulations of LC molecules, which in many cases have large barriers to internal rotation. In this case, we typically modify from 1 to 3 torsional potentials per molecule, reducing the torsional barriers by as much as a factor of 5 in the course of an HMC step. A number of other variants of HMC are possible in the context of molecular simulation, and it is possible to mix different sorts of HMC moves in a given simulation, or mix HMC moves with other types of MC moves (for instance including volume-changing MC moves to generate an *NPT* ensemble). A more detailed discussion of HMC will appear in a forthcoming publication [20].

The requirement that the MD algorithm used in HMC be reversible and area-preserving is, as it turns out, not a disadvantage. In fact, one of the simplest and most widely used MD integration algorithms, the leapfrog integrator [21] (which is equivalent to the familiar Verlet integrators), satisfies these criteria. Unfortunately, it appears to be very difficult, if not impossible, to construct a reversible and area-preserving integrator for systems with constraints (e.g. a molecule with constrained bond lengths). Because constraint dynamics is one of the most commonly used time-saving techniques in molecular simulation, this would appear to be a serious drawback of HMC. Fortunately, a reversible and area-preserving multiple-timestep MD (MTSMD) method (essentially a nested leapfrog integrator) has recently appeared [22, 23], which is at least as efficient as constraint dynamics for molecular simulations [24, 25]. As a consequence of the area-preserving property, both the leapfrog and MTSMD integrators have intrinsic long-term stability, which makes them excellent integrators for both MD and HMC.

In this study, we used a MTSMD scheme with four levels of force evaluation. Nonbonded (van der Waals and Coulombic) forces were evaluated every 6.5 fs (we refer to this as the large integration timestep). Bond stretching forces were evaluated 12 times per large integration timestep (roughly every 0.5 fs), bond angle bending forces were evaluated 6 times per large timestep, and the remaining components of force (dihedral torsion, improper torsion, mean-field, and elongation forces) were evaluated 3 times per large timestep. This scheme was found to be optimal for molecular systems with implicit hydrogens, and is about 50% faster than constraint dynamics [25]. In order to use such a large timestep for systems with explicit hydrogens, we set the hydrogen mass equal to that of carbon. Because the equilibrium properties are independent of mass distribution, this has no effect on the static properties of the system, and enables us to use a significantly larger timestep than would otherwise be dictated by the high frequency of the C–H stretch mode.

The optimization of the HMC algorithm with respect to N_{MD} is discussed in detail elsewhere [20]. For molecular fluids, we find that N_{MD} must be relatively large ($N_{MD} \geq 200$) in order for HMC to be of comparable efficiency to MTSMD. The situation for small N_{MD} is analogous to that for a random walk with a very small stepsize, in that the system does not have time to flow very far through configuration space before the velocities get reset. This leads to poor performance in terms of decorrelation of observables. On the other hand, it does not make sense to make N_{MD} larger than the integrated autocorrelation time for the observable of interest, as this will lead to a greater expenditure of computational effort for the same number of independent measurements. In the simulations described here, we chose $N_{MD} = 400$, which led to integrated autocorrelation times for P ranging from 1 to 8 HMC steps. Each simulation consisted of 20% PVHMC moves and 80% standard HMC moves, which yielded an acceptance rate of ~ 90% in all cases.

We carried out simulations for 28 compounds, displayed in Figure 3, for several values of W_0 and θ^{rel}. Each simulation consisted of an initial conjugate-gradient minimization of the potential energy of the molecule in the external potential ($V_{\text{mf}} + V_{\text{elong}}$), followed by a 2×10^5 MD timestep (500 HMC step) equilibration run and a 2×10^6 MD timestep (5000 HMC step) production run.

Figure 4 displays a number of instantaneous molecular configurations, projected onto the tilt plane, from a simulation of W314, with $W_0 = 0.07$ kcal/mole/Å^2, $\theta_{\text{rel}} = 45°$. Clearly, the molecule explores a wide range of conformations and orientations. Tests of our computational scheme for achiral molecules reveal that the expected symmetries of the conformational and orientational distributions are respected to a good approximation, so we are reasonably confident that we are achieving adequate configurational sampling in our simulations. This conclusion is supported by the observation that our results are essentially independent of initial conditions.

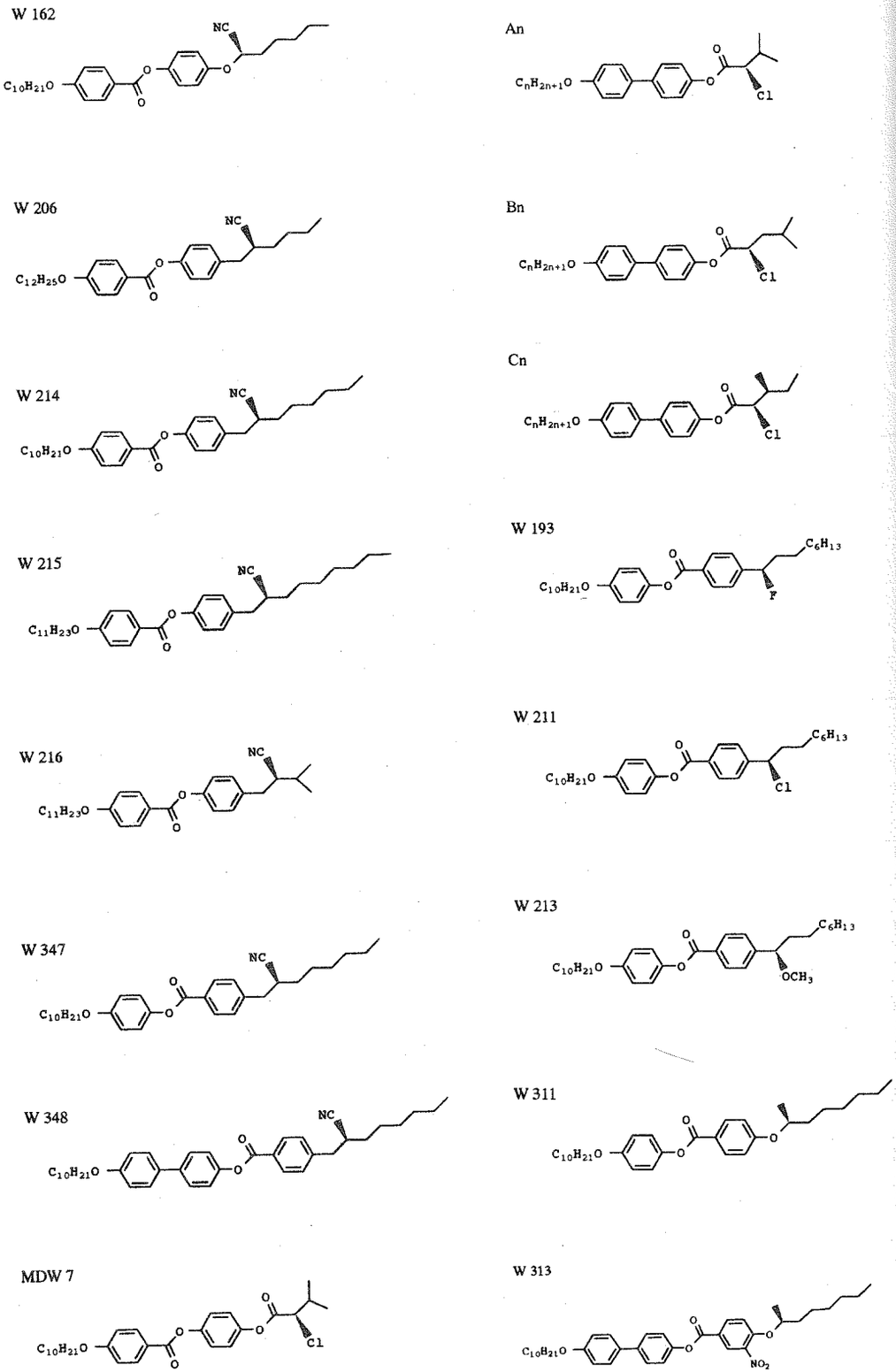

Fig. 3. Chemical structures of the FLC materials studied in this article.

The choice of reasonable values for W_0 and θ_{rel} is of key importance for our calculations. For the purpose of fixing W_0, we made use of C^{13} NMR measurements of orientational order parameters for specific bond segments in several compounds from the homologous series An, Bn, and Cn in the smectic C^* phase [26] (see Figure 3. We performed a series of simulations for a single member of the Cn series, C7, and found that the NMR order parameters were well reproduced for $W_0 = 0.07$ kcal/mole/Å^2,

with $\theta_{rel} = 15°$. This value of W_0 was used for most of the runs reported here. The calculated order parameters depend much less strongly on θ_{rel}, and so the NMR measurements do not serve to constrain this parameter. For this reason, we carried out runs for several different values of θ_{rel}. In all, four series of runs were carried out: for $W_0 = 0.07$ kcal/mole/Å^2, $\theta_{rel} = 15°$, 30°, and 45°, and for $W_0 = 0.06$ kcal/mole/Å^2, $\theta_{rel} = 15°$.

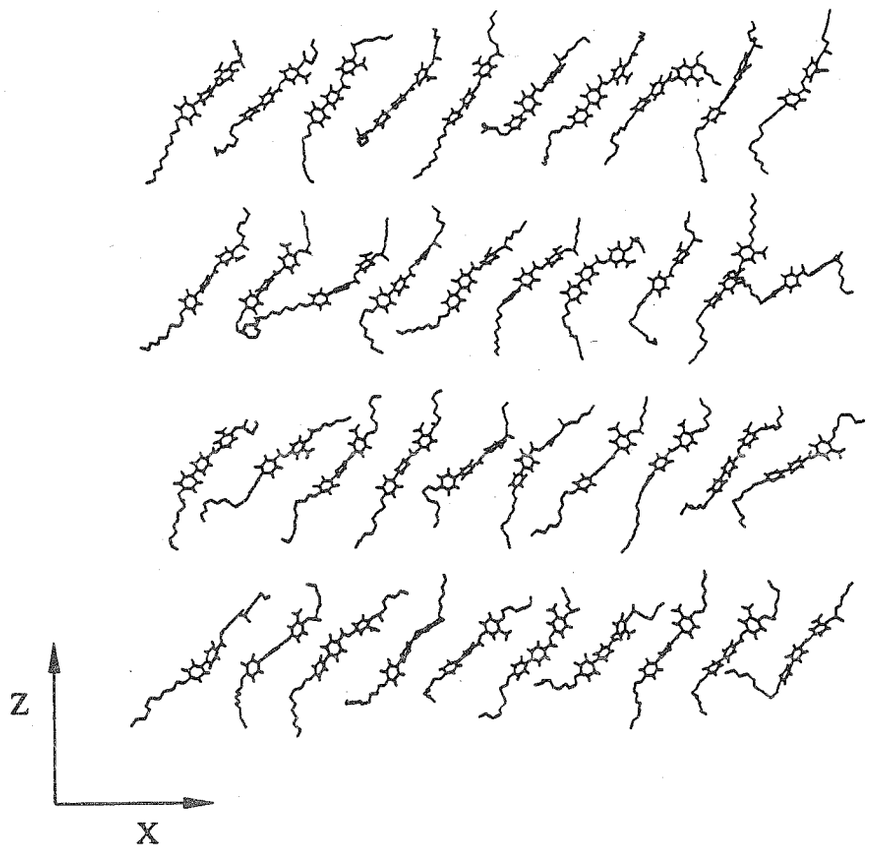

Fig. 4. A series of instantaneous configurations, projected onto the tilt plane, from a mean-field simulation of W314, for $W_0 = 0.07$ kcal/mole/Å^2, $\theta_{rel} = 45°$. This figure gives some indication of the large configuration space sampled by individual molecules in the smectic C^* phase.

The ferroelectric polarization density P is related to the y-component of the average molecular dipole moment $\langle\mu\rangle$ via $P = \rho\langle\mu_y\rangle$, where ρ is the molecular number density. For the compounds studied here, we assumed a mass density of 1 gm/cm^2 in calculating P, which is a reasonably good approximation for most smectic C materials.

Table. Measured and calculated polarization densities for the compounds shown in Figure 3. Calculated polarization densities for four different parameter sets are listed: (1) $W_0 = 0.07$ kcal/mole/Å^2, $\theta_{rel} = 15°$; (2) $W_0 = 0.07$ kcal/mole/Å^2, $\theta_{rel} = 30°$; (3) $W_0 = 0.07$ kcal/mole/Å^2, $\theta_{rel} = 45°$; (4) $W_0 = 0.06$ kcal/mole/Å^2, $\theta_{rel} = 15°$. Temperatures and measured optical tilt angles (where known) are also listed.

Compound	T (°C)	θ_{opt}(°)[a]	P_{exp}(nC/cm^2)[a]	P_{calc}(nC/cm^2)			
				(1)	(2)	(3)	(4)
W162	30	31.5	+98	+23±22	−17±25	−8±24	−16±22
W206	34	–	+111	+46±22	+126±23	+139±22	+36±19
W214	28.3	30.3	+81	+105±21	+167±24	+166±24	+46±20
W215	30	26.8	+24	+80±23	+121±21	+77±23	+36±21
W216	42.3	22.9	+118	+38±20	+58±23	+132±25	+7±21
W347	35	27	+64	+67±26	+89±22	+194±27	+93±21
W348	108.5	–	+121	+65±18	+104±18	+121±19	+56±17
MDW7	30	–	−125	−22±28	−98±27	−112±28	−11±29
A7	71	20	−140	−94±28	−99±27	−105±25	−71±29
A8	66	20	−150	−43±28	−117±27	−178±28	−35±30
A9	61	18	−40	−79±26	−126±29	−173±33	−89±30
B7	53	–	−80	−91±24	−167±25	−160±26	−59±30
C7	44	24	−280	−103±26	−158±28	−196±30	−99±32
C8	37	21	−280	−102±26	−174±30	−219±33	−35±33
C9	43	20	−130	−108±29	−132±29	−199±30	−83±30
W193	38	25.8	+43	+145±30	+305±32	+440±33	+137±34
W211	32	21	+37	+218±47	+391±41	+357±53	+142±43
W213	16.2	20.5	−15	−30±25	−194±36	−72±23	−93±27
W311	10	30.1	+49	+61±21	+54±23	+112±30	+45±21
W313	65	35.2	−305	−202±57	−238±55	−256±68	−123±49
W314	33	32	−426	−303±60	−251±62	−469±70	−116±55
W316	20	25	−252	−202±62	−345±65	−517±75	−138±66
W317	30	25.5	−129	−180±62	−361±63	−390±69	−211±59
W361	108.5	–	−378	−154±56	−249±64	−348±76	−227±61
W363	25	26.5	−870	−273±72	−547±87	−609±98	−231±80
W364	25	31	−718	−200±83	−334±91	−604±96	−233±76
W365	25	30.5	−880	−151±89	−430±81	−584±102	−175±75
W374	70	24.5	−183	−154±47	−257±48	−316±60	−163±47

V. RESULTS AND DISCUSSION

The calculated ferroelectric polarization densities, P_{calc}, for the compounds shown in Figure 3 are listed in Table I, together with the experimentally measured polarization densities, P_{exp} [27, 28]. The experimental values listed are the *saturated* values, i.e. the maximum values of P measured in the smectic C^* phase for the materials in question. Roughly half of the materials studied do not have a smectic C^* phase. The values of P_{exp} listed for these compounds are the *extrapolated* polarization densities

obtained from measurements on mixtures of these compounds with achiral smectic *C* host materials [6]. Also listed in Table I are the optical tilt angles θ_{opt}, where known, which vary from 18° to 35°.

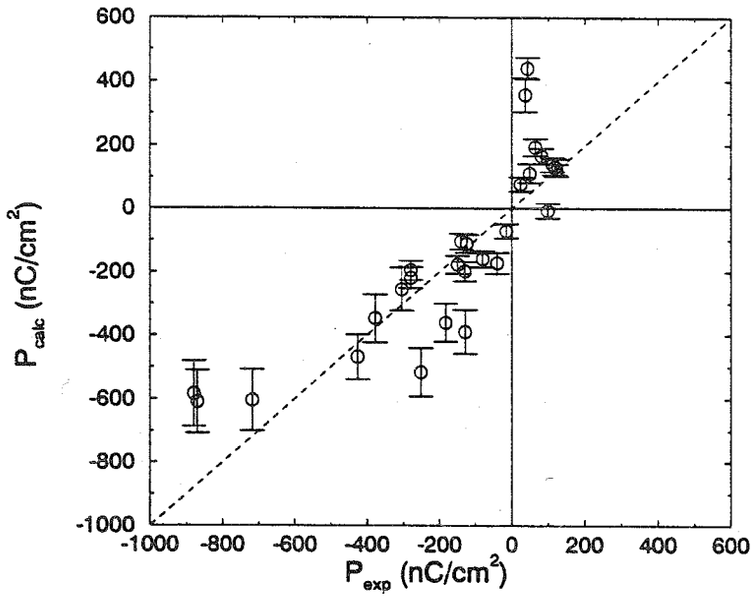

Fig. 5. Scatter plot of P_{exp} vs. P_{calc} (symbols). The dashed line is the line $P_{exp} = P_{calc}$. The experimental and calculated values are reasonably well correlated, although some large deviations from the line $P_{exp} = P_{calc}$ are evident.

In general, our model reproduces qualitative trends in the data well. The correct sign of *P* is observed in almost all cases (the only exception being W162), and a general correlation between the experimental and calculated magnitude of *P* is evident. This can be seen in Figure 5, which is a scatter plot of P_{calc} vs. P_{exp} for $W_0 = 0.07$ kcal/mol/Å^2, $\theta_{rel} = 45°$. There is a clear tendency for the data points to follow the line $P_{calc} = P_{exp}$, although there are some notable deviations, discussed in more detail below.

Several features of the data shown in Table I are worth noting. First of all, we see that the uncertainties in P_{calc} range from 20 nC/cm^2 to 100 nC/cm^2, and generally increase with increasing *P*. This implies that the current method is not well suited to the study of low-*P* materials or to the investigation of small variations of *P* with chemical structure. It is currently feasible for us to reduce the uncertainties in our calculations by a factor of 2 (by carrying out runs that are 4 times as long). In the long run, however, an analytic solution of Equation 6 should be the best way of eliminating statistical uncertainties. Even if statistical uncertainties are eliminated, however, it is clear

that our model is too simple to reproduce many of the observed variations of *P* with molecular structure, if a fixed parametrization of V_{mf} is used. For example, our model is relatively insensitive to changes in the number of methylene groups in the nonchiral tail, and so is not capable of reproducing the strong dependence of *P* on n for the An and Cn homologous series. Our model is also relatively insensitive to subtle changes in the structure of the core, for instance in the series of compounds W313, W314, W316, and W317, in which *P* is experimentally observed to depend strongly on the placement and orientation of the bridging ester group in the core. Both of these effects are collective in nature (reflecting changes in global ordering with molecular structure) and so are not included in the single-molecule theory used here. Although such effects could in principle be accommodated by varying the parameters in V_{mf}, this would require abandoning the universality assumption, and would not be in keeping with the spirit of our approach.

Secondly, it is evident that our model severely overestimates the magnitude of *P* for materials having lateral substituents at the first carbon of an alkyl tail (W193, W211, and W213). This may reflect a deficiency of our current force field, a breakdown of the universality assumption (significantly smaller values for W_0 and/or θ_{rel} may need to be used for these materials), or some more fundamental shortcoming of our model.

Finally, we observe that the spontaneous polarization densities of high-*P* materials (W363, W364, W365) are reproduced by the model only for the largest value of θ_{rel} ($\theta_{rel} = 45°$), and that the best overall agreement between theory and experiment for all compounds is obtained for this value of θ_{rel}. At present, we are unable to judge whether such a large value of θ_{rel} is physically reasonable. The resolution of this issue awaits experimental measurements capable of providing detailed information about the relative orientations of core and tail groups in FLC molecules.

Several factors complicate the interpretation of our results. For one thing, the experimental data listed in Table I were collected under a variety of thermodynamic conditions. In particular, the optical tilt angles vary by almost a factor of 2 for the compounds listed, which makes a uniform comparison of P_{exp} with P_{calc} difficult, since *P* is expected to have a strong dependence on the tilt angle. Moreover, it is not clear how to relate the θ_{rel} of our model to θ_{opt}, since it is not possible to calculate θ_{opt} within the framework of our model. Finally, the experimental measurements themselves are subject to considerable uncertainty. For these reasons, and because the universality assumption necessarily limits the quantitative predictive power of our model, we chose to use raw, saturated polarization densities for purposes of comparison, with the implicit understanding that only semi-quantitative agreement of theory with experiment can be expected.

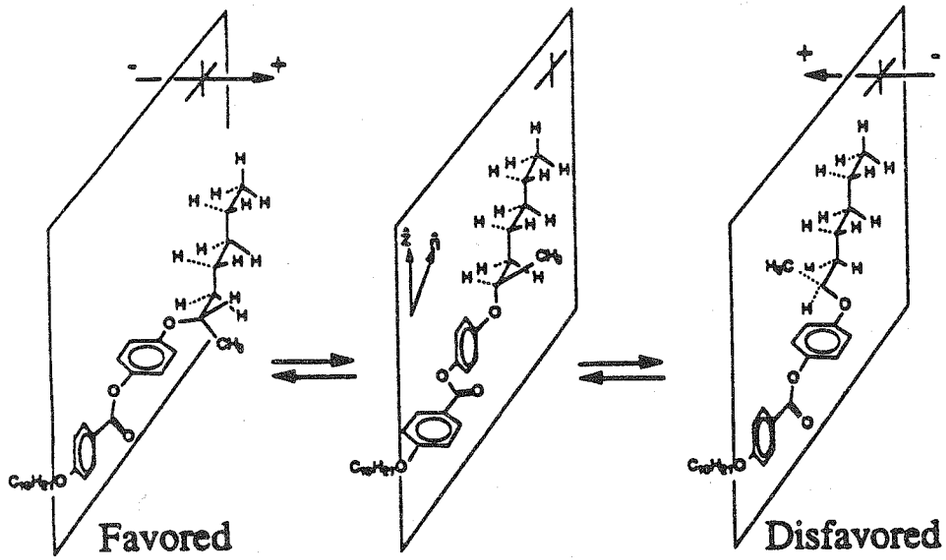

Fig. 6. The three molecular conformations important in the Chisso effect. Conformation A (g^-) is assumed to be energetically preferred relative to conformation C (g^+). This assumption leads to the prediction of a net negative polarization density, arising from the dipole moment of the second bond in the chiral tail. In this picture, the backbone of the chiral tail beyond the second bond is assumed to lie in the tilt plane, with the core more tilted than the tail.

In light of this, the level of agreement between theory and experiment evident in Table I and Figure 5 is impressive, and clearly demonstrates the potential of this approach for yielding semi-quantitative predictions of *P*. More importantly, our results provide strong support for the Boulder model for ferroelectric polarization in FLCs, and cast doubt upon theories that rely on specific chiral interactions to produce ferroelectricity [8]. Moreover, our calculations enable us to examine in detail specific features of the molecular orientational and conformational distributions relevant to the determination of *P*, and to identify those polar groups that make the largest contributions to *P*.

An example of the type of information that our calculations can provide pertains to the so-called "Chisso effect" [6]. This effect has been invoked to rationalize the polarization of materials such as W311. As illustrated by Figure 6, the polarization in this material is thought to arise from an energetic preference for one gauche rotational isomer (g^-) about the γ (third) bond in the chiral tail relative to the g^+ isomer. In this picture, the ferroelectric polarization arises primarily from the bond dipole associated with the second bond in the chiral tail, which has a significant component normal to the tilt plane in the g^- configuration. (The absolute configuration of the compound shown in Figure 6 is opposite to that of W311, and so this argument predicts a negative polarization, whereas W311 has positive polarization. For the same reason, g^+ rather than g^- should be the energetically favoured isomer in W311.) This general picture is supported by 6–31G** calculations [15], which show that the g^- and t isomers are about 1 kcal/mole lower in energy than the g^+ isomer. The question is, how important is this effect, and how is this picture modified by the orienting mean-field potential?

We have measured the fractions of $g^\pm$ and t rotational isomers about the β (second) and γ bonds in W311 for $W_0 = 0.07$ kcal/mole/Å^2, $\theta_{rel} = 45°$, and have found that, as expected, the g^+ isomer about the γ bond is somewhat more probable (33.5%) than the g^- isomer (31.4%). The t isomer is more probable (35.2%) than either gauche isomer. The same behavior is observed for $\theta_{rel} = 30°$, but the situation is reversed for $\theta_{rel} = 15°$, with the g^- isomer being more probable (33.8%) than g^+ (30.6%). The picture thus turns out to be somewhat more complicated than Figure 6 would suggest. When conformations of both the β and γ bonds are considered, it is found that the tg^+ conformation is significantly more probable (31.5%) than the tg^- conformation (17.6%) for $\theta_{rel} = 45°$, in agreement with the Chisso argument (similar behavior is observed for $\theta_{rel} = 15°$ and $\theta_{rel} = 30°$). However, three other conformations are present with significant probability: tt (17.0%), g^- (18.2%), and g^-g^- (13.8%). An analysis of the partial contributions of various conformations to the overall polarization density reveals that the majority contribution to *P* comes from the tg^+ conformation in all cases, as expected from the Chisso argument. Surprisingly, the contribution of the tg^- conformation to *P* is nearly zero, rather than negative. This implies that the orientational ordering of the tg^- conformation is weaker than that of the tg^+ conformation or that the preferred orientation of the tg^- conformation is significantly different from that shown in Figure 6. We have also analyzed individual bond dipole contributions to *P* for W311, and find that the majority contribution to *P* comes from the β bond in the chiral tail, as predicted on the basis of the Chisso argument.

An analogous effect is thought to explain the large polarization densities of nitro-substituted compounds such as W314. In this case, the preference for a specific gauche isomer (here, the g^- isomer) about the γ bond leads to a large contribution to *P* from the nitro group. In the g^- state, the nitro group is rotated out of the tilt plane, and both the nitro and C-O (β bond) dipoles contribute additively (63.9% and 28.6%, respectively, for $W_0 = 0.07$ kcal/mole/Å^2, $\theta_{rel} = 45°$) to the overall polarization. In this case, our results appear to be at variance with the Chisso argument, with the g^+ isomer being significantly more probable (41.2%) than either g^- (31.6%) or t (27.2%). As for W311, however, an examination of conformations of both the β and γ bonds shows that the picture is somewhat more complicated, with 5 important conformations present: tg– (30.3%), tg^+ (28.0%), tt (17.9%), g^+g^+ (13.2%), and g^+t (9.3%). Notice that the tg^- conformation is somewhat more probable than tg^+, in agreement with the simple picture of Figure 6. However, the situation is reversed for $\theta_{rel} = 30°$ and $\theta_{rel} = 15°$.

Nevertheless, we find in all cases that the largest partial contribution to P (~ 50%) comes from the tg^- conformation, as expected from the Chisso argument. The reason for this is somewhat different than that suggested by Figure 6, however, having more to do with the orientational distributions of various conformations than with simple conformational statistics. In fact, we find that the tg^+ conformation makes a *negative* contribution to P, which implies that the preferred orientation of this conformation is quite different from that shown in Figure 6.

On the whole, our results are in accord with our earlier intuition about the origins of ferroelectricity. Only bond dipoles rigidly coupled to the chiral center contribute significantly to P, and the ordering is generally consistent with that inferred from the Boulder model [6]. Clearly, however, our model is capable of revealing new physics (e.g. with regard to the Chisso effect), and should prove to be a powerful tool for designing FLC materials having specific properties. A more detailed description of our results will appear in the near future [29].

VI. CONCLUSIONS

In this article, we have shown that a simple modular mean-field theory for the ferroelectric polarization density in FLCs is capable of yielding semi-quantitative predictions of P, and can give considerable insight into the molecular origins of P. Our findings strongly support the physical mechanism for P embodied in the Boulder model, and cast doubt on theories that invoke specific chiral interactions to produce polar ordering in FLCs.

We are currently working on an analytic version of our theory, which should enable us to carry out more systematic studies for a much wider variety of materials. We have also initiating work on cluster approximations for realistic liquid crystal models in an attempt to include intermolecular interactions and correlations in a direct way.

Models of this type have a much wider range of applicability than has been indicated here. We plan to extend our theory to the modelling of NMR and FTIR spectra of LCs, and to the calculations of linear and nonlinear optical properties of LCs.

We would like to thank Demetri Photinos for numerous helpful suggestions. This work was supported by the National Science Foundation Materials Synthesis and Processing Program Grant DMR-9202312 and by the National Science Foundation Materials Research Group Grant DMR-9224168.

(Received 13 April 1995)

References

[1] M. P. Allen, G. T. Evans, D. Frenkel, B. M. Mulder, Adv. Chem. Phys. **86**, 1 (1993).
[2] M. A. Glaser, R. Malzbender, N. A. Clark, D. M. Walba, to be published in Molecular Simulation (1995); M. A. Glaser, R. Malzbender, N. A. Clark, and D. M. Walba, J. Phys.: Condens. Matter **6**, A261 (1994); S. Ye. Yakovenko, A. A. Minko, G. Krömer and A. Geiger, Liq. Cryst. **17**, 127 (1994); M. R. Wilson and M. P. Allen, Liq. Cryst. **12**, 157 (1992); M. R. Wilson and M. P. Allen, Mol. Cryst. Liq. Cryst. **198**, 465 (1991); I. Ono and S. Kondo, Mol. Cryst. Liq. Cryst. Lett. **8**, 69 (1991); B. Jung and B. L. Schürmann, Mol. Cryst. Liq. Cryst. **185**, 141 (1990); S. J. Picken, W. F. van Gunsteren, P. Th. van Duijnen and W. H. de Jeu, Liq. Cryst. **6**, 357 (1989); A. V. Komolkin, Yu. V. Molchanov, and P. P.Yakutseni, Liq. Cryst. **6**, 39 (1989).
[3] R. B. Meyer, L. Liébert, L. Strzelecki, P. Keller, J. Phys. (Paris) Lett. **36**, 69 (1975).
[4] N. A. Clark and S. T. Lagerwall, Appl. Phys. Lett. **36**, 899 (1980).
[5] P. G. de Gennes, *The Physics of Liquid Crystals* (Oxford University Press, London, 1975).
[6] D. M. Walba, in *Advances in the Synthesis and Reactivity of Solids* (JAI Press, Ltd., 1991), Vol. 1, p. 173.
[7] R. Bartolino, J. Doucet, and G. Durand, Ann. Phys. **3**, 389 (1978).
[8] S. A. Pikin and M. A. Osipov, in *Ferroelectric Liquid Crystals: Principles, Properties, and Applications*, ed. J. Goodby (Gordon and Breach, Philadelphia, 1991), p. 249.
[9] D. J. Photinos and E. T. Samulski, preprint (1995).
[10] D. J. Photinos, E. T. Samulski, H. Toriumi, Mol. Cryst. Liq. Cryst. **204**, 161 (1991).
[11] S. Marcelja, J. Chem. Phys. 60, 3599 (1974).
[12] G. R. Luckhurst, Mol. Phys. **82**, 1063 (1994).
[13] J. I. Siepmann, S. Karaborni, B. Smit, Nature **365**, 330 (1993).
[14] X. Shi and L. S. Bartell, J. Phys. Chem. **92**, 5667 (1988).
[15] E. Garcia, M. A. Glaser, D. M. Walba, N. A. Clark, in preparation.
[16] S. Duane, A. D. Kennedy, B. J. Pendleton, D. Roweth, Phys. Lett. B **195**, 216 (1987).
[17] See B. M. Forrest and U. W. Suter, J. Chem. Phys. **101**, 2616 (1994), and references therein.
[18] W. G. Hoover, Phys. Rev. A **31**, 1685 (1985).
[19] D. Kusnezov, A. Bulgac, W. Bauer, Ann. Phys. **204**, 155 (1990).
[20] M. A. Glaser, D. Frenkel, N. A. Clarc, in preparation.
[21] M. P. Allen and D. J. Tildesley, *Computer Simulation of Liquids* (Clarendon, Oxford, 1987).
[22] M. Tuckermann, B. J. Berne, G. J. Martyna, J. Chem. Phys. **97**, 1990 (1992).
[23] J. C. Sexton and D. H. Weingarten, Nucl. Phys. B **380**, 665 (1992).
[24] M. Watanabe and M. Karplus, J. Chem. Phys. **99**, 8063 (1993).
[25] M. A. Glaser, D. Frenkel, N. A. Clark, in preparation.
[26] M.-S. Ho, B. M. Fung, M. Wand, R. T. Vohra, *Ferroelectrics* **138**, 51 (1993); C.-D. Poon and B. M. Fung, J. Chem. Phys. **91**, 7392 (1989); C.-D. Poon and B. M. Fung, Liq. Cryst. **5**, 1159 (1989).
[27] Data from the FLC Materials Research Group, Boulder, Colorado.
[28] Ch. Bahr and G. Heppke, Mol. Cryst. Liq. Cryst. Lett. **4**, 31 (1986); Ch. Bahr and G. Heppke, Mol. Cryst. Liq. Cryst. **148**, 29 (1987); K. Yoshino, M. Ozaki, S.-I. Kishio, T. Sakurai, N. Mikami, R.-I. Higuchi, M. Honma, Mol. Cryst. Liq. Cryst. **144**, 87 (1987).
[29] M. A. Glaser, V. V. Ginzburg, N. A. Clark, E. Garcia, D. M. Walba, and R. Malzbender, in preparation.